Cell Reports

Inhibitory Control of Feature Selectivity in an Object Motion Sensitive Circuit of the Retina

Graphical Abstract

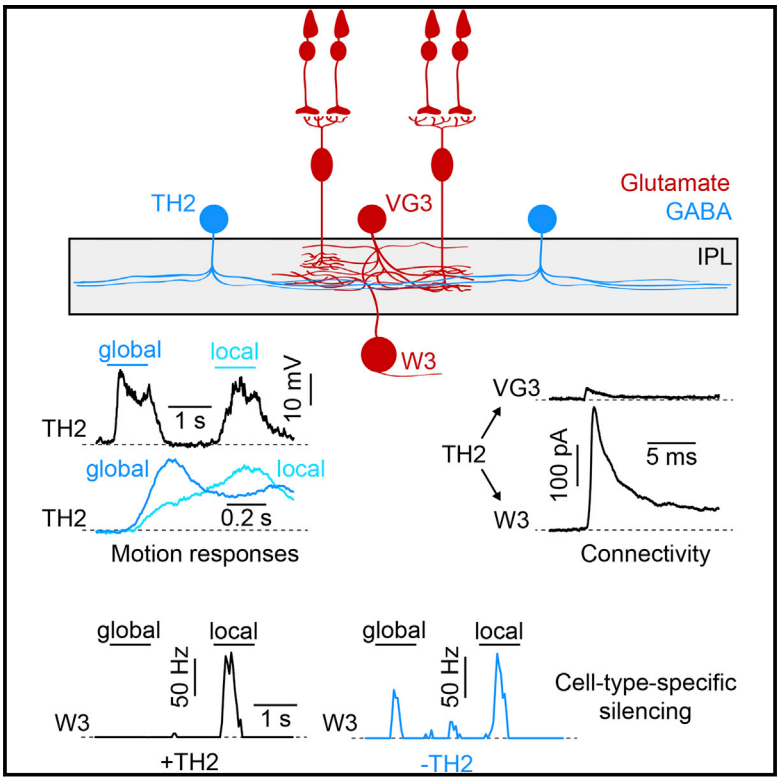

Highlights

- TH2-ACs are a genetically identifiable wide-field amacrine cell type in mice
- TH2-ACs distinguish global and local motion stimuli in their response timing
- TH2-ACs provide strong GABAergic input to object motion sensitive W3-RGCs
- Inhibitory input from TH2-ACs suppresses W3-RGC responses to global motion stimuli

Authors

Tahnbee Kim, Daniel Kerschensteiner

Correspondence

kerschensteinerd@wustl.edu

In Brief

Kim and Kerschensteiner report that a specific amacrine cell type (TH2-AC) distinguishes local and global motion in the kinetics of its responses. Optogenetic activation and cell-type-specific silencing show that TH2-ACs provide strong inhibitory input to object motion sensitive retinal ganglion cells (W3-RGCs) and that this input suppresses W3-RGC responses to global motion stimuli.

Kim & Kerschensteiner, 2017, Cell Reports *19*, 1343–1350
May 16, 2017
http://dx.doi.org/10.1016/j.celrep.2017.04.060

CellPress

Cell Reports
Report

Inhibitory Control of Feature Selectivity in an Object Motion Sensitive Circuit of the Retina

Tahnbee Kim[1,2] and Daniel Kerschensteiner[1,3,4,5,6,*]
[1]Department of Ophthalmology and Visual Sciences
[2]Graduate Program in Neuroscience
[3]Department of Neuroscience
[4]Department of Biomedical Engineering
[5]Hope Center for Neurological Disorders
Washington University School of Medicine, Saint Louis, MO 63110, USA
[6]Lead Contact
*Correspondence: kerschensteinerd@wustl.edu
http://dx.doi.org/10.1016/j.celrep.2017.04.060

SUMMARY

Object motion sensitive (OMS) W3-retinal ganglion cells (W3-RGCs) in mice respond to local movements in a visual scene but remain silent during self-generated global image motion. The excitatory inputs that drive responses of W3-RGCs to local motion were recently characterized, but which inhibitory neurons suppress W3-RGCs' responses to global motion, how these neurons encode motion information, and how their connections are organized along the excitatory circuit axis remains unknown. Here, we find that a genetically identified amacrine cell (AC) type, TH2-AC, exhibits fast responses to global motion and slow responses to local motion. Optogenetic stimulation shows that TH2-ACs provide strong $GABA_A$ receptor-mediated input to W3-RGCs but only weak input to upstream excitatory neurons. Cell-type-specific silencing reveals that temporally coded inhibition from TH2-ACs cancels W3-RGC spike responses to global but not local motion stimuli and, thus, controls the feature selectivity of OMS signals sent to the brain.

INTRODUCTION

In many parts of the nervous system, the diversity of inhibitory interneurons exceeds that of excitatory projection neurons (Freund and Buzsáki, 1996; Tasic et al., 2016). In part because of this diversity, the function of many interneurons remains unknown, and the organization of inhibitory circuits is not well understood (Isaacson and Scanziani, 2011). The diversity of interneurons may be greatest in the retina, which in mice contains approximately 50 types of amacrine cells (ACs) (Helmstaedter et al., 2013; MacNeil and Masland, 1998). Each AC type studied so far has a different task in vision, and as a population, ACs support the encoding of diverse visual features in the spike trains of approximately 40 retinal ganglion cell (RGC) types, which send retinal information to the brain (Euler et al., 2002; Grimes et al., 2010; Jacoby et al., 2015; Kim et al., 2015; Vlasits et al., 2014; Yoshida et al., 2001; Hoggarth et al., 2015; Dacheux and Raviola, 1986; Chen and Li, 2012; Baden et al., 2016). ACs can shape the output of RGCs directly through input to their dendrites (i.e., postsynaptic inhibition) or indirectly through synapses on bipolar cell axons or other ACs (i.e., presynaptic inhibition) (Demb and Singer, 2015; Franke et al., 2017). The contributions of most AC types to visual processing remain unknown. In addition, it is unclear whether individual AC types preferentially provide pre- or postsynaptic inhibition or equally inhibit multiple components of the same circuit.

Detecting the movements of objects (e.g., an attacking predator) is an essential function of visual systems, and object motion strongly attracts attention (Abrams and Christ, 2003) and can elicit innate defensive behaviors in prey species (De Franceschi et al., 2016; Yilmaz and Meister, 2013). To reliably signal object motion, neural circuits need to distinguish it from self-generated motion (e.g., eye movements) (Olveczky et al., 2003). In the retinal image, object- and self-generated motion causes local and global displacements, respectively. In mice, W3-RGCs receive excitatory input from bipolar cells and from VGluT3-expressing ACs (VG3-ACs) (Krishnaswamy et al., 2015; Kim et al., 2015; Lee et al., 2014). Local motion depolarizes bipolar cells and VG3-ACs and elicits robust spiking in W3-RGCs, but during global motion, these neurons are silenced (Kim et al., 2015; Zhang et al., 2012). Global motion evokes inhibitory input to all three tiers of the excitatory circuit axis via the axons of bipolar cells, the neurites of VG3-ACs, and the dendrites of W3-RGCs (Kim et al., 2015; Krishnaswamy et al., 2015; Lee et al., 2014; Zhang et al., 2012). Which AC types provide this inhibitory input, how they distinguish local and global motion, and whether a single AC type preferentially targets a single tier of the excitatory circuit axis or provides similar input to all of them is unknown.

Recent anatomical work showed that the neurites of a genetically identified AC type, TH2-AC, co-stratify with and appear to contact dendrites of W3-RGCs and neurites of VG3-ACs in the inner plexiform layer (IPL) (Brüggen et al., 2015; Knop et al., 2011). Here, using targeted patch-clamp recordings, optogenetic circuit mapping, and cell-type-specific silencing, we identify a critical function of TH2-ACs in object motion encoding in the retinal output.

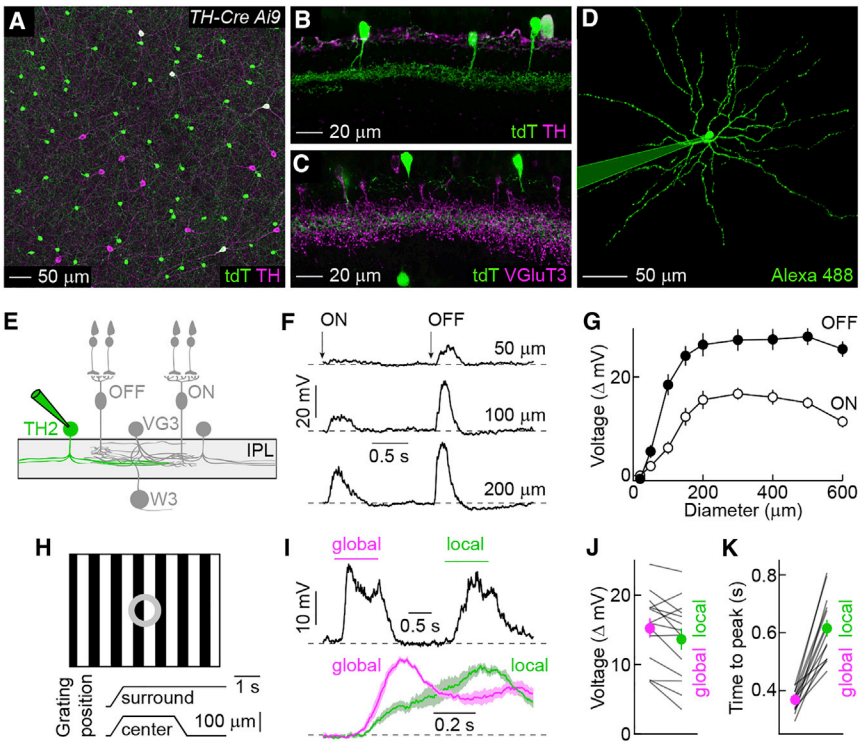

Figure 1. Genetically Identified TH2-ACs Distinguish Local and Global Motion in Their Response Timing

(A) Representative image of the INL of a flat-mounted *TH-Cre Ai9* retina stained for tdT and TH.

(B and C) Vibratome sections of *TH-Cre Ai9* retinas stained for tdT and TH (B) or VGluT3 (C).

(D) An individual TH2-AC filled with Alexa 488 via a patch-clamp electrode targeted under two-photon guidance.

(E) Schematic illustration of the W3-RGC circuit (ON and OFF bipolar cells, VG3-ACs, and W3-RGCs) and TH2-ACs.

(F and G) Representative traces (F) and summary data (G) (mean ± SEM, n = 12) of voltage responses of TH2-ACs to a stimulus in which intensity in spots of varying diameters was square wave-modulated (1.5 s ON, 1.5 s OFF).

(H) Schematic illustrating motion stimulus. Two square wave gratings (bar width 50 µm, contrast 100%) one covering the center and one the surround of the excitatory circuit axis, are separated by a gray annulus. During stimulus presentation, both gratings first move together (i.e., global motion), and then the center grating moves alone (i.e., local motion).

(I) A representative voltage response of a TH2-ACs to the stimulus illustrated in (H) is presented in the top graph. Mean ± SEM of responses of TH2-ACs (n = 14) to global (magenta) and local (green) stimuli aligned on the respective motion onsets are shown by lines (shaded areas) in the bottom graph.

(J and K) Individual (gray lines) and population (mean ± SEM, circles with error bars) data comparing response amplitudes (J) (n = 14, p = 0.016) and timing (K) ($p = 1.2 \times 10^{-4}$) to global (magenta) and local (green) motion stimuli.

See also Figures S1 and S2.

RESULTS

Temporal Distinction of Local versus Global Motion by Genetically Identified TH2-ACs

We crossed mice in which an 11 kb fragment of the tyrosine hydroxylase (TH) promoter drives expression of Cre recombinase (*TH-Cre*) to a fluorescent reporter strain (*Ai9*) (Savitt et al., 2005; Madisen et al., 2010). In the inner nuclear layer (INL) of *TH-Cre Ai9* mice, a dense population of TH-negative cells expressed tdTomato (tdT), in addition to sparse subsets of dopaminergic ACs (DACs, TH-positive) and starburst ACs (SACs) (Figures 1A and S1) (Vuong et al., 2015). The cell bodies of the dense TH-negative population were arranged in regular mosaics, indicating that they belonged to a single cell type (Figure S1). Neurites of this cell type stratified in the center of the IPL, where they overlapped with neurites of VG3-ACs (Figures 1B, 1C, and S1). Under two-photon guidance, we targeted the dense population in the INL for patch-clamp recordings and filled individual cells with an intracellular dye, revealing wide-field neurite arborizations (Figures 1D, 1E, and S1). Together with the genetic labeling and stratification patterns, this identified the dense TH-negative population as TH2-ACs (Knop et al., 2011; Vuong et al., 2015). Consistent with a previous study (Knop et al., 2011), we found that TH2-ACs depolarized to light increments (ON) and decrements (OFF) over a wide range of stimulus sizes (Figures 1F and 1G). Responses of TH2-ACs to visual motion had not yet been explored. Given co-stratification with object motion sensitive (OMS) circuits in the middle of the IPL (Figures 1B, 1C, and S1) (Brüggen et al., 2015; Jacoby and Schwartz, 2017; Knop et al., 2011), we tested responses of TH2-ACs to global and local motion stimuli previously used to characterize VG3-ACs and W3-RGCs (Figure 1H) (Zhang et al., 2012; Kim et al., 2015). TH2-ACs depolarized with slightly larger amplitudes to global than local motion (Figures 1I and 1J). More striking than differences in amplitudes, however, were differences in response kinetics to these motion stimuli. Whereas global motion elicited fast depolarizations, responses to local motion were much slower (Figures 1I and 1K). These differences in response kinetics persisted across a variety of stimulus contrasts (Figure S2). Thus, TH2-ACs appear to distinguish object- and self-generated movements predominantly in their response timing. Intriguingly, similar differences in kinetics have been observed in the inhibitory inputs to VG3-ACs and W3-RGCs, with fast surround inhibition canceling excitatory center inputs during global motion (Kim et al., 2015; Zhang et al., 2012).

Optogenetic Exploration of Inhibition from TH2-ACs to VG3-ACs and W3-RGCs

We used optogenetics to test if TH2-ACs provide input to VG3-ACs and/or W3-RGCs and to analyze what transmitter(s) and receptor(s) mediate this putative communication. We first recorded TH2-ACs expressing channelrhodopsin 2 fused to yellow

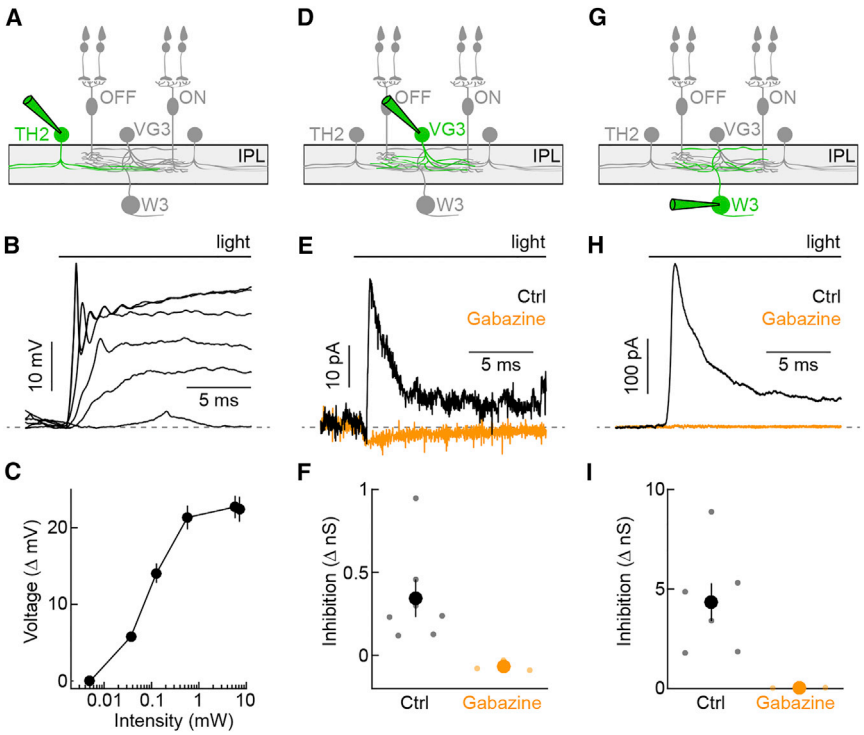

Figure 2. Optogenetic Mapping of TH2-AC Connectivity

(A, D, and G) Schematics illustrating the W3-RGC circuit with cell type recorded in the graphs below (A, TH2-AC; D, VG3-AC; G, W3-RGC) highlighted (green).

(B and C) Representative traces (B) and summary data (C) (mean ± SEM, n = 6) of TH2-AC voltage responses to increasing optogenetic stimulus intensities presented in a 2-mm-diameter spot (*TH-Cre Ai32*). To map connectivity, stimuli of 0.57 mW were used.

(E and F) Representative traces (E) and summary data (F) of IPSCs (V_{hold} = 0 mV) recorded in VG3-ACs during optogenetic stimulation of TH2-ACs (*TH-Cre VG3-Cre Ai32*) in the control conditions (black) and in the presence of gabazine (orange). In (F), each dot represents data from individual cells, and the larger circles (error bars) indicate the mean ± SEM of the respective populations (control n = 7, gabazine n = 4, p = 0.006).

(H and I) Analogous to (E) (H) and (F) (I), but for IPSCs recorded from W3-RGCs (*TH-Cre Ai32*, control n = 7, gabazine n = 3, p = 0.016). TH2-AC-driven IPSCs are approximately 10-fold larger in W3-RGCs than in VG3-ACs ($p = 5.8 \times 10^{-4}$).

fluorescent protein (ChR2-YFP) to identify stimulus parameters that matched optogenetic depolarizations to those observed during photoreceptor-driven light responses (Figures 2A–2C; *TH-Cre Ai32*) (Park et al., 2015; Tien et al., 2016). In all optogenetic experiments, the transmission of photoreceptor signals to bipolar cells and excitatory synaptic transmission in the inner retina were blocked by inclusion of L-AP4 (20 μM), ACET (10 μM), D-AP5 (30 μM), and NBQX (40 μM) in the extracellular solution (Park et al., 2015; Tien et al., 2016). We obtained patch-clamp recordings from VG3-ACs in mice in which both TH2-ACs and VG3-ACs (for targeting) express ChR2-YFP (Figure 2D; *TH-Cre VG3-Cre Ai32*). Holding VG3-ACs at 0 mV (the reversal potential of ChR2-mediated currents) allowed us to isolate inhibitory synaptic inputs. Optogenetic stimulation reliably elicited small inhibitory postsynaptic currents (IPSCs) in VG3-ACs (Figures 2E and 2F), which were not observed in mice in which only VG3-ACs express ChR2-YFP (data not shown; *VG3-Cre Ai32*). These IPSCs were blocked by application of the $GABA_A$ receptor antagonist gabazine (Figures 2E and 2F). In W3-RGCs, optogenetic stimulation elicited approximately 10-fold larger IPSCs than in VG3-ACs, which were equally blocked by gabazine (Figures 2G and 2H; *TH-Cre Ai32*). Thus, TH2-ACs preferentially inhibit the final tier of the excitatory circuit axis, providing strong $GABA_A$ receptor-mediated input to W3-RGCs and only weak $GABA_A$ receptor-mediated input to VG3-ACs.

Cell-Type-Specific Silencing of TH2-ACs Selectively Reduces Inhibitory Input to W3-RGCs

To reveal the contributions of TH2-ACs to visual processing, we endeavored to silence them in a cell-type-specific manner. We crossed *TH-Cre* mice to a conditional knockout strain of the vesicular GABA transporter (*VGATcKO*) (Tong et al., 2008). We used optogenetics to confirm that this manipulation suppressed inhibitory transmission from TH2-ACs. Indeed, VGAT deletion greatly reduced IPSCs in W3-RGCs without affecting the optogenetic activation of TH2-ACs (Figure S3; *TH-Cre VGATcKO Ai32* versus *TH-Cre Ai32*). The small residual IPSCs we observed in a subset of our recordings may be the result of incomplete Cre expression in the population of TH2-ACs and electrical coupling between TH2-ACs (Brüggen et al., 2015). We next analyzed how TH2-AC silencing affected photoreceptor-driven inhibition in VG3-ACs and W3-RGCs. Stationary ON and OFF stimuli of increasing size elicited increasing IPSCs in VG3-ACs. These IPSCs were unaffected by VGAT deletion in TH2-ACs (Figures 3A–3C; *TH-Cre VG3-Cre VGATcKO Ai9* versus *TH-Cre VG3-Cre Ai9*). In contrast, TH2-AC silencing reduced inhibitory inputs to W3-RGCs evoked by the same stimulus to less than half their normal amplitudes (Figures 3D–3F; *TH-Cre VGATcKO* versus *TH-Cre*). Given the limited overlap of DAC and SAC neurites with OMS circuits in the middle of the IPL (Figure S1), and the fact that only sparse subsets of DACs and SACs are labeled in *TH-Cre* mice (Figure S1), it is unlikely that they contribute significantly to our findings. Interestingly, light responses of TH2-ACs themselves were largely unaffected by deletion of VGAT and by removal of VGluT3 (Figure S4; *TH-Cre VGATcKO Ai9* and *TH-Cre VGluT3KO Ai9* versus *TH-Cre Ai9*), and no IPSCs were observed in TH2-ACs following optogenetic stimulation of TH2-ACs and VG3-ACs (data not shown; *TH-Cre VG3-Cre Ai32*). Together these results indicate that TH2-ACs do not inhibit one another, or receive input from VG3-ACs, or provide much output to them. Instead, TH2-ACs dominate surround inhibition to W3-RGCs.

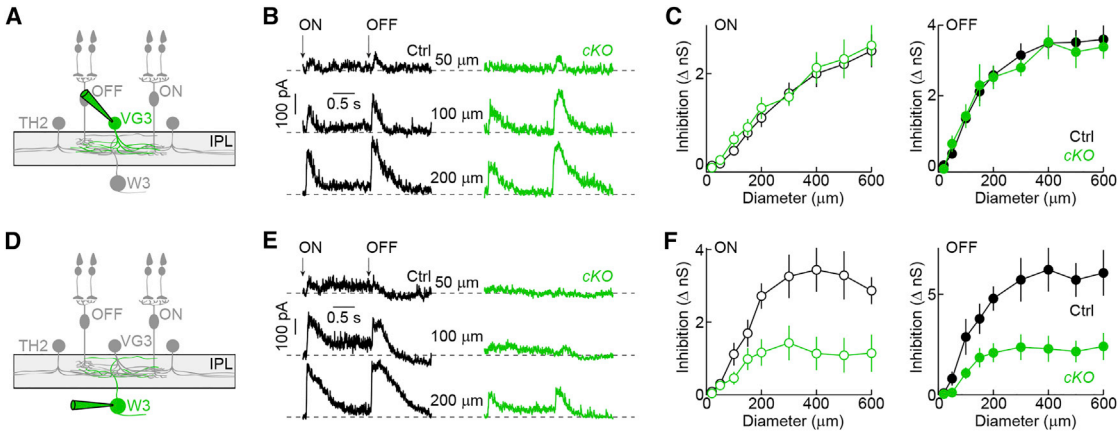

Figure 3. Silencing of TH2-ACs Reveals Preferential Inhibition to the W3-RGCs

(A and D) Schematic illustrating the W3-RGC circuit with the cell type recorded in the graphs to the right (A, VG3-AC; D, W3-RGC) highlighted (green).

(B and C) Representative traces (B) and summary data (C) (mean ± SEM) of VG3-AC IPSCs elicited stationary ON and OFF stimuli of increasing size (i.e., spot diameter). Recordings from mice in which TH2-ACs lack VGAT (*TH-Cre VG3-Cre VGATcKO Ai9* [cKO], green, n = 10) and control mice (*TH-Cre VG3-Cre Ai9*, black [Ctrl], n = 24,) are compared (ON, p = 0.94; OFF, p = 0.902).

(E and F) Analogous to (B) (E) and (C) (F) but for recordings of IPSCs in W3-RGCs, which are reduced when TH2-ACs are silenced (*TH-Cre VGATcKO* [cKO], green, n = 13) compared with when TH2-ACs are active (*TH-Cre* [Ctrl], black, n = 10; ON, p = 0.012; OFF, p = 0.006).

See also Figures S3 and S4.

Cell-Type-Specific Silencing of TH2-ACs Reduces Feature Selectivity of OMS Signals to the Brain

To analyze the impact of TH2-ACs on motion processing, we compared global and local motion responses along the excitatory circuit axis between mice in which TH2-ACs were silenced and control littermates. Because of surround inhibition onto bipolar cell axons, excitatory inputs to VG3-ACs are smaller during global than local motion (Kim et al., 2015). This preference for local motion, summarized by a local motion preference index (LMPI; Experimental Procedures), was unchanged when TH2-ACs were silenced, indicating that TH2-ACs do not inhibit the bipolar cell axons in this circuits (Figures 4A–4C; *TH-Cre VG3-Cre VGATcKO Ai9* versus *TH-Cre VG3-Cre Ai9*). Similarly, inhibitory inputs to VG3-ACs elicited by local and global motion were unchanged (Figures 4D and 4E), consistent with our results from stationary stimuli (Figures 3B and 3C), and voltage differences between VG3-ACs' depolarizations to local motion and hyperpolarizations to global motion were preserved (Figures 4F and 4G). Because we observed no change in the bipolar cell input to VG3-ACs and in their voltage responses, we expected the excitatory input from bipolar cells and VG3-ACs to W3-RGCs to be unaltered as well. Indeed, excitatory synaptic conductances in W3-RGCs showed equal local motion preference in mice in which TH2-ACs were silenced and in control littermates (Figures 4H–4J; *TH-Cre VGATcKO* versus *TH-Cre*). In contrast, inhibitory inputs to W3-RGCs elicited by global motion were drastically reduced by VGAT deletion in TH2-ACs (*TH-Cre*: 2.02 ± 0.2 nS, n = 17; *TH-Cre VGATcKO*: 0.8 ± 0.16 nS, n = 12; p = 1.8×10^{-4}), resulting in a switch in motion preference (Figures 4K and 4L). As a consequence of this reduced surround inhibition, W3-RGCs spiked robustly during global motion when TH2-ACs were silenced (*TH-Cre*: 2 ± 0.2 Hz, n = 17; *TH-Cre VGATcKO*: 18.6 ± 4.1 Hz, n = 17; p = 0.0019), and the near perfect object motion selectivity of output signals from W3-RGCs to the brain was lost (Figures 4M and 4N).

DISCUSSION

We find that TH2-ACs, a genetically identified type of wide-field ACs (Vuong et al., 2015; Knop et al., 2011), distinguish local and global motion primarily in the speed of their responses (Figure 1). This temporal code of TH2-ACs was similarly observed in responses to stationary stimuli (Knop et al., 2011) and likely reflects the recruitment of voltage-dependent conductances that speed up depolarizations with increasing stimulus strengths. Response kinetics were unaffected by tetrodotoxin (TTX) (data not shown), arguing that TTX-sensitive voltage-gated sodium channels, which accelerate responses of other ACs (Tian et al., 2010), do not contribute to temporal coding in TH2-ACs. Previously observed effects of TTX on global motion suppression of VG3-ACs and W3-RGCs (Zhang et al., 2012; Kim et al., 2015) thus either reflect local effects on synaptic transmission from TH2-ACs not evident in recordings from their soma and/or are accounted for by actions on other AC types contributing to surround inhibition in the W3-RGC circuit.

VGAT deletion in TH2-ACs drastically reduced inhibitory input to W3-RGCs during global but not during local motion (Figure 4), suggesting that the fast responses of TH2-ACs to global motion drive transmitter release more effectively than slow responses of similar amplitude during local motion. Several mechanisms, including calcium channel inactivation, activity of calcium extrusion pumps, and vesicle pool dynamics, may contribute to this differential transmission (Demb and Singer, 2015; Grant and Fuchs, 2008; Morgans et al., 1998). In addition to effective transmission, fast responses ensure that the inhibitory output of TH2-ACs coincides with and cancels excitatory inputs to W3-RGCs

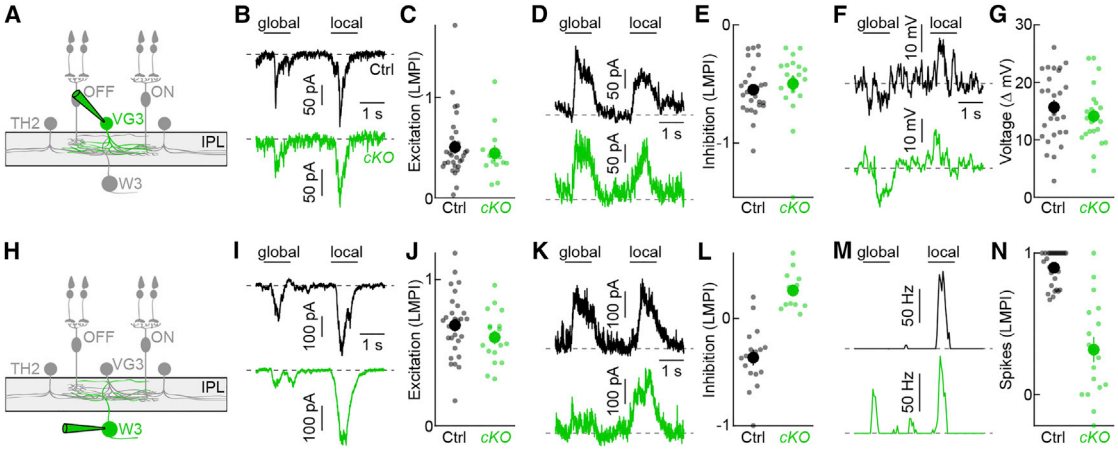

Figure 4. Silencing of TH2-ACs Reduces Feature Selectivity of OMS Signals to the Brain

(A and H) Schematic illustrating the W3-RGC circuit with the cell type recorded in the graphs to the right (A, VG3-AC; H, W3-RGC) highlighted (green).

(B and C) Representative traces of excitatory input to VG3-ACs during global and local motion (B) and summary data of a local motion preference index (LMPI) (C) compared between mice in which TH2-ACs lack VGAT (*TH-Cre VG3-Cre VGATcKO Ai9* [cKO], green, n = 13) and control mice (*TH-Cre VG3-Cre Ai9* [Ctrl], black, n = 30, p = 0.57). In (C), each dot represents data from individual cells, and the larger circles (error bars) indicate the mean ± SEM of the respective populations.

(D and E) Analogous to (B) (D) and (C) (E), but for inhibitory inputs to VG3-ACs (*TH-Cre VG3-Cre VGATcKO Ai9* [cKO], green, n = 19; *TH-Cre VG3-Cre Ai9* [Ctrl], black, n = 27, p = 0.14).

(F and G) Representative traces of VG3-AC voltage responses during global and local motion (F) and summary data of the difference between both responses (G) compared between mice in which TH2-ACs lack VGAT (*TH-Cre VG3-Cre VGATcKO Ai9* [cKO], green, n = 22) and control mice (*TH-Cre VG3-Cre Ai9* [Ctrl], black, n = 27, p = 0.43).

(I and J) Representative traces of excitatory input to W3-RGCs during global and local motion (I) and LMPI summary data (J) compared between mice in which TH2-ACs lack VGAT (*TH-Cre VGATcKO* [cKO], green, n = 17) and control mice (*TH-Cre* [Ctrl], black, n = 28, p = 0.18).

(K and L) Analogous to (I) (K) and (J) (L) but for inhibitory inputs to W3-RGCs (*TH-Cre VGATcKO* [cKO], green, n = 12; *TH-Cre* [Ctrl], black, n = 17, $p = 3.5 \times 10^{-5}$).

(M and N) Analogous to (I) (M) and (J) (N) but for spike responses of W3-RGCs (*TH-Cre VGATcKO* [cKO], green, n = 17; *TH-Cre* [Ctrl], black, n = 30, $p = 1.1 \times 10^{-6}$).

during global motion, whereas slower inhibition during local motion peaks after excitation (Zhang et al., 2012; Baccus et al., 2008; Kim et al., 2015). Thus, the temporal code of TH2-ACs is translated into feature-selective inhibition.

Inhibition occurs on three tiers of the excitatory axis via bipolar cell axons, VG3-AC neurites, and W3-RGC dendrites (Kim et al., 2015; Lee et al., 2014; Zhang et al., 2012). We find that TH2-ACs preferentially inhibit W3-RGCs, suppress their spike responses to global motion, and thus control the feature selectivity of OMS signals sent to the brain (Figures 2 and 4). Although optogenetic stimulation of TH2-ACs elicited small IPSCs in VG3-ACs (Figure 2), silencing of TH2-ACs showed no deficits at this or the preceding tier (Figures 3 and 4), arguing that presynaptic inhibition is dominated by other AC types. Interestingly, in salamanders, a group of polyaxonal ACs was shown to provide presynaptic inhibition in an OMS circuit (Baccus et al., 2008). Whether homologous ACs serve a similar function in mammalian retinas, and to what extent the selectivity for pre- or postsynaptic inhibition is common among AC types remains to be determined.

We previously posited that if multiple AC types converge in the same circuit, they each make distinct and separable contributions to the overall computation (Tien et al., 2016). In the W3-RGC circuit, VG3-ACs selectively amplify responses to local motion (Kim et al., 2015), whereas TH2-ACs selectively suppress responses to global motion (Figure 4), highlighting this organizing principle. Other examples include the division of labor among AC types that inhibit suppressed-by-contrast RGCs during stimuli of different size and contrast (Tien et al., 2015, 2016; Jacoby et al., 2015; Lee et al., 2016) and between AC types that underlie the direction and size selectivity, respectively, of direction-selective RGCs (Hoggarth et al., 2015).

In addition to convergence, signals of AC types can diverge and may exert similar influences on multiple targets. It is tempting to speculate that in addition to W3-RGCs, TH2-ACs may contribute to surround inhibition of a recently identified group of RGCs that stratify in the center of the IPL and that like W3-RGCs track movements of small objects (Jacoby and Schwartz, 2017).

EXPERIMENTAL PROCEDURES

Animals

Throughout our study, we used various combinations of the following mouse strains: *VG3-Cre* (Grimes et al., 2010), provided by Dr. R. H. Edward; *TH-Cre* (Savitt et al., 2005), from The Jackson Laboratory (RRID: IMSR_JAX:008601); *Ai9* (Madisen et al., 2010), from The Jackson Laboratory (stock #007909); *Ai32* (Madisen et al., 2012), from The Jackson Laboratory (stock #012569); *VGATcKO* (Tong et al., 2008), from The Jackson Laboratory (stock #012897); and *VGluT3KO* (Seal et al., 2008), from The Jackson Laboratory (stock #016931). Mice were housed in a 12 hr light/dark cycle and fed ad libitum. We isolated retinas from mice of both sexes aged between postnatal day 20 (P20) and postnatal day 40 (P40) and compared littermates with appropriate genotypes in control and experimental groups. All experiments in this study were approved by the Institutional Animal Care and Use Committee of Washington University School of Medicine and were performed in compliance with the National Institutes of Health *Guide for the Care and Use of Laboratory Animals*.

Tissue Preparation

Mice were dark adapted for >2 hr, deeply anesthetized with CO_2, killed by cervical dislocation, and enucleated. For electrophysiology, retinas were isolated in bicarbonate-buffered mACSF ($mACSF_{NaHCO3}$) containing 125 mM NaCl, 2.5 mM KCl, 1 mM $MgCl_2$, 1.25 mM NaH_2PO_4, 2 mM $CaCl_2$, 20 mM glucose, 26 mM $NaHCO_3$ and 0.5 mM L-glutamine equilibrated with 95% O_2/5% CO_2 and flat-mounted on transparent membrane discs (Anodisc, Whatman). For anatomy, retinas were isolated in HEPES-buffered mACSF ($mACSF_{HEPES}$) containing 119 mM NaCl, 2.5 mM KCl, 2.5 mM $CaCl_2$, 1.3 mM $MgCl_2$, 1 mM NaH_2PO_4, 11 mM glucose, and 20 mM HEPES (pH adjusted to 7.37 with NaOH) and flat mounted on black membrane discs (HABGO1300, Millipore). All procedures were carried out under infrared illumination.

Electrophysiology

Patch-clamp recordings from TH2-ACs, VG3-ACs, and W3-RGCs were obtained in the dorsal halves of retinal flat-mount preparations continually perfused (~8 mL/min) with warm (33°C) $mACSF_{NaHCO3}$ (Kim et al., 2015; Wang et al., 2011). TH2-ACs and VG3-ACs were targeted under two-photon guidance in transgenic retinas in which these cells are fluorescently labeled. W3-RGCs were approached under conventional infrared illumination. Cell type identities were confirmed by characteristic neurite arbor morphologies visualized by two-photon imaging of Alexa 488 (1 mM) included in the intracellular solution at the end of each recording. In addition, W3-RGCs were distinguished from other small RGCs by their longer response latencies to small spots of light (Jacoby and Schwartz, 2017). The intracellular solution for current-clamp recordings contained: 125 mM K-gluconate, 10 mM NaCl, 1 mM $MgCl_2$, 10 mM EGTA, 5 mM HEPES, 5 mM ATP-Na, and 0.1 mM GTP-Na (pH adjusted to 7.2 with KOH). The intracellular solution for voltage-clamp recordings contained: 120 mM Cs-gluconate, 1 mM $CaCl_2$, 1 mM $MgCl_2$, 10 mM Na-HEPES, 11 mM EGTA, 10 mM TEA-Cl, and 2 mM Qx314 (pH adjusted to 7.2 with CsOH). Patch pipettes had resistances of 4–7 MΩ (borosilicate glass). Signals were amplified with a Multiclamp 700B amplifier (Molecular Devices), filtered at 3 kHz (eight-pole Bessel low-pass) and sampled at 10 kHz (Digidata 1440A, Molecular Devices). In voltage-clamp recordings, series resistance (10–15 MΩ) was compensated electronically by ~75%. Excitatory postsynaptic currents (EPSCs) and IPSCs were isolated by holding cells at the reversal potential of inhibitory (−60 mV) and excitatory (0 mV) conductances, respectively. In current-clamp recordings, no bias current was injected. In recordings of optogenetic responses, the transmission of photoreceptor signals to bipolar cells and excitatory synaptic transmission in the inner retina were blocked by addition of L-AP4 (Tocris, 20 μM), ACET (Tocris, 10 μM), D-AP5 (Tocris, 30 μM), and NBQX (Tocris, 40 μM) to the $mACSF_{NaHCO3}$. In a subset of recordings, gabazine (SR-95531, Sigma-Aldrich, 10 μM) was added to the $mACSF_{NaHCO3}$ to block $GABA_A$ receptors.

Visual Stimulation

Visual stimuli written in MATLAB (The MathWorks) were presented on an organic light-emitting display (OLED-XL, eMagin) using Cogent graphics extensions (John Romaya, Laboratory of Neurobiology, Wellcome Department of Imaging Neuroscience, University College London) and were projected onto the photoreceptors of the retina via the substage condenser of an upright two-photon microscope (FV1000 MPE, Olympus). All stimuli were centered on the soma of the recorded cells, and their average intensity was kept constant at ~1,500 rhodopsin isomerizations/rod/s. To measure the size preference of TH2-ACs, VG3-ACs, and W3-RGCs, the intensity of spots of varying diameter was square wave-modulated at 0.333 Hz (1.5 s ON, 1.5 s OFF) for five cycles (Michelson contrast 96%). The order in which spots of different size were presented was randomly chosen for each cell, and the first stimulus in the sequence repeated at its end to confirm stability of the recording. To test responses to object versus global motion stimuli, narrow square wave gratings (bar width 50–75 μm) over the receptive field center and surround were moved separately or in unison (Kim et al., 2015; Zhang et al., 2012). A gray annulus was included in the spatial layout of the stimulus to reliably separate movement in the center and surround.

Optogenetics

To activate ChR2, light from a mercury bulb (Olympus) was band-pass filtered (426–446 nm, Chroma) and projected onto the RGC side of the retina (spot diameter 2 mm) through a 20× 0.9 NA objective on an upright two-photon microscope (FV1000 MPE). Intensity of the optogenetic stimulus was varied by inserting different neutral density filters into its path, and a Uniblitz shutter (Vincent Associates) controlled stimulus timing.

Immunohistochemistry

Eye cups or flat-mounted retinas were fixed for 30 min in 4% paraformaldehyde (PFA) in $mACSF_{HEPES}$ at room temperature (RT) and washed three times for 10 min in PBS at RT. For vibratome sections (thickness 60 μm), retinas were isolated from eye cups, embedded in agarose and cut (VT1000P, Leica), and then stained. Flat-mounted retinas were cryoprotected with a series of 10%, 20%, and 30% sucrose in PBS for 1 hr (at RT), 1 hr (at RT), and overnight (at 4°C), respectively. The tissue then underwent three cycles of freezing (held over liquid nitrogen) and thawing (in 30% sucrose in PBS), was washed three times in PBS for 10 min at RT, and was subsequently stained. The following primary antibodies were in different combinations: rabbit anti-TH (EMD Millipore, 1:1,000), rabbit anti-VGluT3 (Synaptic Sytems, 1:1,000), goat anti-ChAT (EMD Millipore, 1:500), and mouse anti-tdT (Abcam, 1:1,000). Retinas were incubated with primary antibodies in PBS with 5% normal donkey serum and 0.5% Triton X-100 for 3–5 days (flat mounts) or overnight (sections) at 4°C. Subsequently, they were washed three times for 10 min in PBS, stained with Alexa 488-, Alexa 568-, and/or Alexa 633-conjugated secondary antibodies (Invitrogen, 1:1,000) overnight at 4°C (flat mounts) or 1 hr at RT (sections). The tissue was then washed three times in PBS for 10 min and mounted in Vectashield mounting medium (Vector Laboratories).

Confocal and Two-Photon Imaging

Confocal image stacks of fixed tissue were acquired through 20× 0.85 NA or 60× 1.35 NA oil immersion objectives (Olympus) on an upright microscope (FV1000, Olympus). The voxel sizes of confocal image stacks ranged from 0.62–1 μm (x/y − z) to 0.1–0.3 μm (x/y − z). Two-photon image stacks of neurons filled with Alexa 488 during patch-clamp recordings were acquired through a 20× 0.9 NA water immersion objective (Olympus) on an upright microscope (FV1000 MPE) at a voxel size of 0.62–1 μm (x/y − z).

Analysis of Electrophysiology Data

Response amplitudes to visual and optogenetic stimuli were measured as baseline-subtracted averages during 100–200 ms time windows. To compare responses to local and global motion stimuli, we computed a local motion preference index as

$$LMPI = \frac{R_L - R_G}{R_L + R_G},$$

where R_L and R_G indicate responses to local and global motion stimuli, respectively. For VG3-AC voltage recordings, we measured the difference between responses to local and global motion, rather than the LMPI, to avoid division by small denominators. Electrophysiology data were processed and analyzed using scripts written in MATLAB.

Analysis of Imaging Data

To analyze the density and distribution of cells labeled in *TH-Cre Ai9* retinas, flat mounts were co-stained for tdTomato (tdT), choline acetyltransferase (ChAT), and TH. In agreement with previous studies (Knop et al., 2011; Vuong et al., 2015), we identified TH2-ACs as the cells that are positive for tdT but negative for ChAT and TH. By contrast, SACs are ChAT positive, and DACs are TH positive. Soma positions of TH2-ACs were marked manually in projections of confocal image stacks through the INL and ganglion cell layer (GCL) and density recovery profiles calculated according to Rodieck (1991). Imaging data were processed and analyzed using Fiji (Schindelin et al., 2012) and scripts written in MATLAB.

Statistical Tests

To compare single value measurements between groups, we used Wilcoxon rank sum tests. To compare response amplitudes to increasing spot sizes between two groups (e.g., different genotypes), we used bootstrapping with

10,000 replicates. Differences in the actual average response curves were compared with differences of average response curves when data were randomly assigned to the compared groups.

SUPPLEMENTAL INFORMATION

Supplemental Information includes four figures and can be found with this article online at http://dx.doi.org/10.1016/j.celrep.2017.04.060.

AUTHOR CONTRIBUTIONS

Experiments were designed by T.K. and D.K. Experiments were conducted by T.K. Data were analyzed by T.K. and D.K. The manuscript was written by T.K. and D.K.

ACKNOWLEDGMENTS

We thank members of the Kerschensteiner lab for helpful comments and suggestions throughout this study. This work was supported by the NIH (EY023341, EY026978, and EY027411 to D.K. and the Vision Core Grant EY0268) and by an unrestricted grant from the Research to Prevent Blindness Foundation to the Department of Ophthalmology and Visual Sciences at Washington University.

Received: February 17, 2017
Revised: April 15, 2017
Accepted: April 20, 2017
Published: May 16, 2017

REFERENCES

Abrams, R.A., and Christ, S.E. (2003). Motion onset captures attention. Psychol. Sci. *14*, 427–432.

Baccus, S.A., Olveczky, B.P., Manu, M., and Meister, M. (2008). A retinal circuit that computes object motion. J. Neurosci. *28*, 6807–6817.

Baden, T., Berens, P., Franke, K., Román Rosón, M., Bethge, M., and Euler, T. (2016). The functional diversity of retinal ganglion cells in the mouse. Nature *529*, 345–350.

Brüggen, B., Meyer, A., Boven, F., Weiler, R., and Dedek, K. (2015). Type 2 wide-field amacrine cells in TH:GFP mice show a homogenous synapse distribution and contact small ganglion cells. Eur. J. Neurosci. *41*, 734–747.

Chen, S., and Li, W. (2012). A color-coding amacrine cell may provide a blue-off signal in a mammalian retina. Nat. Neurosci. *15*, 954–956.

Dacheux, R.F., and Raviola, E. (1986). The rod pathway in the rabbit retina: a depolarizing bipolar and amacrine cell. J. Neurosci. *6*, 331–345.

De Franceschi, G., Vivattanasarn, T., Saleem, A.B., and Solomon, S.G. (2016). Vision guides selection of freeze or flight defense strategies in mice. Curr. Biol. *26*, 2150–2154.

Demb, J.B., and Singer, J.H. (2015). Functional circuitry of the retina. Annu. Rev. Vision Sci. *1*, 263–289.

Euler, T., Detwiler, P.B., and Denk, W. (2002). Directionally selective calcium signals in dendrites of starburst amacrine cells. Nature *418*, 845–852.

Franke, K., Berens, P., Schubert, T., Bethge, M., Euler, T., and Baden, T. (2017). Inhibition decorrelates visual feature representations in the inner retina. Nature *542*, 439–444.

Freund, T.F., and Buzsáki, G. (1996). Interneurons of the hippocampus. Hippocampus *6*, 347–470.

Grant, L., and Fuchs, P. (2008). Calcium- and calmodulin-dependent inactivation of calcium channels in inner hair cells of the rat cochlea. J. Neurophysiol. *99*, 2183–2193.

Grimes, W.N., Zhang, J., Graydon, C.W., Kachar, B., and Diamond, J.S. (2010). Retinal parallel processors: more than 100 independent microcircuits operate within a single interneuron. Neuron *65*, 873–885.

Helmstaedter, M., Briggman, K.L., Turaga, S.C., Jain, V., Seung, H.S., and Denk, W. (2013). Connectomic reconstruction of the inner plexiform layer in the mouse retina. Nature *500*, 168–174.

Hoggarth, A., McLaughlin, A.J., Ronellenfitch, K., Trenholm, S., Vasandani, R., Sethuramanujam, S., Schwab, D., Briggman, K.L., and Awatramani, G.B. (2015). Specific wiring of distinct amacrine cells in the directionally selective retinal circuit permits independent coding of direction and size. Neuron *86*, 276–291.

Isaacson, J.S., and Scanziani, M. (2011). How inhibition shapes cortical activity. Neuron *72*, 231–243.

Jacoby, J., and Schwartz, G.W. (2017). Three small-receptive-field ganglion cells in the mouse retina are distinctly tuned to size, speed, and object motion. J. Neurosci. *37*, 610–625.

Jacoby, J., Zhu, Y., DeVries, S.H., and Schwartz, G.W. (2015). An amacrine cell circuit for signaling steady illumination in the retina. Cell Rep. *13*, 2663–2670.

Kim, T., Soto, F., and Kerschensteiner, D. (2015). An excitatory amacrine cell detects object motion and provides feature-selective input to ganglion cells in the mouse retina. eLife *4*, 4.

Knop, G.C., Feigenspan, A., Weiler, R., and Dedek, K. (2011). Inputs underlying the ON-OFF light responses of type 2 wide-field amacrine cells in TH:GFP mice. J. Neurosci. *31*, 4780–4791.

Krishnaswamy, A., Yamagata, M., Duan, X., Hong, Y.K., and Sanes, J.R. (2015). Sidekick 2 directs formation of a retinal circuit that detects differential motion. Nature *524*, 466–470.

Lee, S., Chen, L., Chen, M., Ye, M., Seal, R.P., and Zhou, Z.J. (2014). An unconventional glutamatergic circuit in the retina formed by vGluT3 amacrine cells. Neuron *84*, 708–715.

Lee, S., Zhang, Y., Chen, M., and Zhou, Z.J. (2016). Segregated glycine-glutamate Co-transmission from vGluT3 amacrine cells to contrast-suppressed and contrast-enhanced retinal circuits. Neuron *90*, 27–34.

MacNeil, M.A., and Masland, R.H. (1998). Extreme diversity among amacrine cells: implications for function. Neuron *20*, 971–982.

Madisen, L., Zwingman, T.A., Sunkin, S.M., Oh, S.W., Zariwala, H.A., Gu, H., Ng, L.L., Palmiter, R.D., Hawrylycz, M.J., Jones, A.R., et al. (2010). A robust and high-throughput Cre reporting and characterization system for the whole mouse brain. Nat. Neurosci. *13*, 133–140.

Madisen, L., Mao, T., Koch, H., Zhuo, J.M., Berenyi, A., Fujisawa, S., Hsu, Y.W., Garcia, A.J., 3rd, Gu, X., Zanella, S., et al. (2012). A toolbox of Cre-dependent optogenetic transgenic mice for light-induced activation and silencing. Nat. Neurosci. *15*, 793–802.

Morgans, C.W., El Far, O., Berntson, A., Wässle, H., and Taylor, W.R. (1998). Calcium extrusion from mammalian photoreceptor terminals. J. Neurosci. *18*, 2467–2474.

Olveczky, B.P., Baccus, S.A., and Meister, M. (2003). Segregation of object and background motion in the retina. Nature *423*, 401–408.

Park, S.J., Borghuis, B.G., Rahmani, P., Zeng, Q., Kim, I.J., and Demb, J.B. (2015). Function and Circuitry of VIP+ Interneurons in the Mouse Retina. J. Neurosci. *35*, 10685–10700.

Rodieck, R.W. (1991). The density recovery profile: a method for the analysis of points in the plane applicable to retinal studies. Vis. Neurosci. *6*, 95–111.

Savitt, J.M., Jang, S.S., Mu, W., Dawson, V.L., and Dawson, T.M. (2005). Bcl-x is required for proper development of the mouse substantia nigra. J. Neurosci. *25*, 6721–6728.

Schindelin, J., Arganda-Carreras, I., Frise, E., Kaynig, V., Longair, M., Pietzsch, T., Preibisch, S., Rueden, C., Saalfeld, S., Schmid, B., et al. (2012). Fiji: an open-source platform for biological-image analysis. Nat. Methods *9*, 676–682.

Seal, R.P., Akil, O., Yi, E., Weber, C.M., Grant, L., Yoo, J., Clause, A., Kandler, K., Noebels, J.L., Glowatzki, E., et al. (2008). Sensorineural deafness and seizures in mice lacking vesicular glutamate transporter 3. Neuron *57*, 263–275.

Tasic, B., Menon, V., Nguyen, T.N., Kim, T.K., Jarsky, T., Yao, Z., Levi, B., Gray, L.T., Sorensen, S.A., Dolbeare, T., et al. (2016). Adult mouse cortical

cell taxonomy revealed by single cell transcriptomics. Nat. Neurosci. *19*, 335–346.

Tian, M., Jarsky, T., Murphy, G.J., Rieke, F., and Singer, J.H. (2010). Voltage-gated Na channels in AII amacrine cells accelerate scotopic light responses mediated by the rod bipolar cell pathway. J. Neurosci. *30*, 4650–4659.

Tien, N.W., Pearson, J.T., Heller, C.R., Demas, J., and Kerschensteiner, D. (2015). Genetically identified suppressed-by-contrast retinal ganglion cells reliably signal self-generated visual stimuli. J. Neurosci. *35*, 10815–10820.

Tien, N.W., Kim, T., and Kerschensteiner, D. (2016). Target-specific glycinergic transmission from VGluT3-expressing amacrine cells shapes suppressive contrast responses in the retina. Cell Rep. *15*, 1369–1375.

Tong, Q., Ye, C.P., Jones, J.E., Elmquist, J.K., and Lowell, B.B. (2008). Synaptic release of GABA by AgRP neurons is required for normal regulation of energy balance. Nat. Neurosci. *11*, 998–1000.

Vlasits, A.L., Bos, R., Morrie, R.D., Fortuny, C., Flannery, J.G., Feller, M.B., and Rivlin-Etzion, M. (2014). Visual stimulation switches the polarity of excitatory input to starburst amacrine cells. Neuron *83*, 1172–1184.

Vuong, H.E., Pérez de Sevilla Müller, L., Hardi, C.N., McMahon, D.G., and Brecha, N.C. (2015). Heterogeneous transgene expression in the retinas of the TH-RFP, TH-Cre, TH-BAC-Cre and DAT-Cre mouse lines. Neuroscience *307*, 319–337.

Wang, Y.V., Weick, M., and Demb, J.B. (2011). Spectral and temporal sensitivity of cone-mediated responses in mouse retinal ganglion cells. J. Neurosci. *31*, 7670–7681.

Yilmaz, M., and Meister, M. (2013). Rapid innate defensive responses of mice to looming visual stimuli. Curr. Biol. *23*, 2011–2015.

Yoshida, K., Watanabe, D., Ishikane, H., Tachibana, M., Pastan, I., and Nakanishi, S. (2001). A key role of starburst amacrine cells in originating retinal directional selectivity and optokinetic eye movement. Neuron *30*, 771–780.

Zhang, Y., Kim, I.J., Sanes, J.R., and Meister, M. (2012). The most numerous ganglion cell type of the mouse retina is a selective feature detector. Proc. Natl. Acad. Sci. U S A *109*, E2391–E2398.